Measurement of the Tensor Asymmetry A_{zz} from $0.3 < x < 1.9$ and Elastic T_{20}

A Proposal to Jefferson Lab PAC 43
(Update to LOI12-14-002)

E. Long, [†] [‡] K. Slifer,[†] P. Solvignon,[†] T. Badman, R. Zielinski
University of New Hampshire, Durham, NH 03861

D. Crabb, D. Day,[†] D. Keller,[†] S. Liuti, O. A. Rondon, V. Sulkosky
University of Virginia, Charlottesville, VA 22903

A. Camsonne, D. Gaskell, D. Higinbotham[†]
Thomas Jefferson National Accelerator Facility, Newport News, VA 23606

Z. Ye
Duke University, Durham, NC 27708

N. Kalantarians
Hampton University, Hampton, VA 23668

A. Ahmidouch, S. Danagoulian
North Carolina A&T State University, Greensboro, NC 27411

M. Sargsian
Florida International University, Miami, FL 33199

M. Strikman
Pennsylvania State University, University Park, PA 16802

G. Miller
University of Washington, Seattle, WA 98195

[†]Spokesperson
[‡]Contact: ellie@jlab.org

Abstract

In this update to LOI12-14-002, we propose the first measurement of the tensor asymmetry A_{zz} in the quasi-elastic region through the tensor polarized D(e, e')X channel; an asymmetry that is sensitive to the nucleon-nucleon potential. Previous measurements of A_{zz} have been used to extract b_1 in the DIS region and T_{20} in the elastic region. In the quasi-elastic region, A_{zz} data will be used to compare light cone calculations with variation nucleon-nucleon calculations, and is an important quantity to determine for understanding tensor effects, such as the dominance of pn correlations in nuclei.

A_{zz} was first calculated in 1988 by Frankfurt and Strikman, using the Hamada-Johnstone and Reid soft-core wave functions [1]. Recent calculations by M. Sargsian and M. Strikman revisit A_{zz} in the $x > 1$ range using virtual-nucleon and light-cone methods, which differ by up to a factor of two [2] and can be discriminated experimentally at the $3 - 6\sigma$ level. Additionally, the calculations were done using multiple deuteron wavefunctions which show a large discrepancy at high x.

Additionally, our measurement of A_{zz} allows for a simultaneous measurement of the tensor analyzing power T_{20} without any further beam time or equipment by making a kinematic cut on the elastic peak. The lowest Q^2 measurement will fall on the most experimentally probed and theoretically understood region, making it ideal for ensuring that the tensor polarized target is operating correctly and to help reduce target systematic uncertainty, the leading systematic in this experiment. At medium Q^2, our measurement will fall in the same region where there is currently a discrepancy between Hall A and Hall C results. Our final point will lie at the highest Q^2 value ever measured for T_{20}, and will test whether the observable continues on a plateau. These measurements of T_{20} will also cover the largest range in Q^2 measured by a single experiment.

We propose an experimental determination of A_{zz} and T_{20} utilizing the same equipment as the E13-12-011 b_1 experiment. Three different Q^2 values will be measured over the course of 34 days, with 10.3 additional days of overhead. The measurements are less sensitive to systematic uncertainties than E13-12-011, so this experiment would be utilized in parallel to better understand the in-beam conditions and time-dependent systematic effects of a tensor polarized target for the b_1 experiment.

Additionally, the kinematic requirements of A_{zz} also allow for the simultaneous measurement of T_{20} at multiple Q^2 points ranging from $0.13 < Q^2 < 1.8$ GeV^2, the largest range of a single experiment. At low $Q^2 \sim 0.15$ GeV^2, t_{20} is well known experimentally and theoretically making it an ideal calibration point to reduce systematics from target polarization. At mid $Q^2 \sim 0.7$ GeV^2, we will take a measurement in the region where recent JLab Hall C data disagrees with data from Hall A. Finally, at high $Q^2 \sim 1.8$ GeV^2 we will measure T_{20} at the largest momentum transfer yet, further constraining calculations at high Q^2.

Contents

1 A_{zz} Background

The deuteron is the simplest composite nuclear system, and in many ways it is as important to understanding bound states in QCD as the hydrogen atom was to understanding bound systems in QED. Our experimental and theoretical understanding of the deuteron remains unsatisfying.

Due to their small size and simple structure, tensor polarized deuterons are ideal for studying nucleon-nucleon interactions. Tensor polarization enhances the D-state contribution, which compresses the deuteron [3], making the system more sensitive to short-range QCD effects. Understanding the nucleon-nucleon potential of the deuteron is essential for understanding short-range correlations as they are largely dependent on the tensor force [4]. We can resolve the short-range structure of nuclei on the level of nucleon and hadronic constituents by utilizing processes that transfer to the nucleon constituents both energy and momentum larger than the scale of the NN short-range correlations, particularly at $Q^2 > 1\ (\mathrm{GeV}/c)^2$.

By taking a ratio of cross sections from electron scattering from tensor-polarized and unpolarized deuterons, the S and D-wave states can be disentangled, leading to a fuller understanding of the repulsive nucleon core. A measurement of A_{zz} is sensitive to the $\frac{D^2-SD}{S^2+D^2}$ ratio and it's evolution with increasing minimal momentum of the struck nucleon. Originally calculated by L. Frankfurt and M. Strikman [1], this has recently been revisited by M. Sargsian, who calculated A_{zz} in this region using a light cone approach and a virtual nucleon approach. The calculations vary by up to a factor of 2, and can be experimentally determined at the $3-6\sigma$ level as discussed in this letter.

For the lower Q^2 region, W. Van Orden has calculations in progress using different nucleon-nucleon potentials, as well as different prescriptions for handling the reactions mechanisms [5]. Similar calculations are currently being finalized for the approved D$(e,e'p)n$ at high Q^2, high p_m experiment. Once completed, he will turn his attention to tensor polarization observables in the low Q^2 region.

Additionally, measuring A_{zz} in the quasi-elastic region will fill a gap in measurements performed on tensor polarized deuterium. It is directly proportional to the observable used in the elastic region to measure T_{20}, by $A_{zz} \propto T_{20}$. Due to the large acceptance of the SHMS spectrometer, we will be taking data in the $x = 2$ elastic range as well that, at low Q^2, may be able to resolve the discrepancy of the deuteron structure functions that were measured at JLab in Halls A and C [6]. This will be investigated further as a potential parasitic measurement when the full proposal is submitted. In the deep inelastic region, A_{zz} will soon be measured to extract the tensor structure function b_1 by the relation $A_{zz} \propto \frac{b_1}{F_1^D}$. Not only will measuring A_{zz} in the quasi-elastic region provide information necessary for understanding the properties of the deuteron and contribution from the tensor force, but it will be the first experiment to bridge a gap in measurements of electron scattering from tensor-polarized deuterons.

1.1 Probing the Deuteron Wavefunction

It was suggested for some time [7] that to resolve the microscopic structure of nuclei one needs to study scattering at sufficiently large momentum transfer and large relative momenta of the produced nucleons. This logic was confirmed [4] by a series of experiments at SLAC [8] and

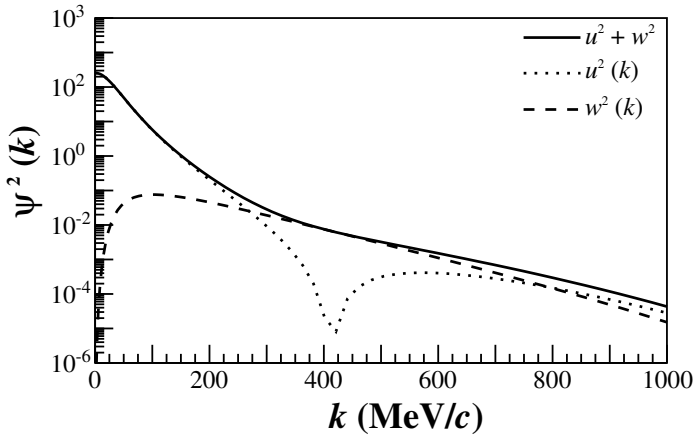

Figure 1: The AV18 [11] deuteron wave-function, showing the dominance of the D-state (dashed) in comparison to the S-state (dotted) in the full wavefunction (solid) at high momentum ($k > 300$ Mev$/c$).

JLab [9, 10] that directly observed short-range correlations (SRC) in a series of nuclei, and established a similar effect of SRC in the deuteron and in heavier nuclei with pn correlations giving the dominant contribution. Hence, the deuteron serves as a "hydrogen atom" for the studies of the microscopic short-range structure of the nuclei since it is the simplest nuclei that follows SRC scaling.

To achieve further progress, it is necessary to improve our knowledge of the deuteron wave function at high momenta, and to separate the S and D contributions to the high momentum component of the deuteron. The dominance of the D-wave at a large range of the nucleon momenta is expected in a range of the theoretical models, as demonstrated in Fig. 1, but experimentally it was probed in a rather indirect way via measurement of T_{20} for the deuteron form factor [6]. Still, the knowledge of S/D ratio for large momenta is rather poor. Indeed, all wavefunctions are constrained by low energy data to reproduce the S/D ratio at small momenta while the overall probability of the D-wave in the deuteron differs by a factor up to 1.5, leading to a large difference of the S/D ratio at large momenta.

The S and D-states are related to the tensor asymmetry A_{zz} by [1]

$$A_{zz} \propto \frac{\frac{1}{2}w^2(k) - u(k)w(k)\sqrt{2}}{u^2(k) + w^2(k)}, \tag{1}$$

where $u(k)$ is the S-state wave function and $w(k)$ is the D-state wave function. Additionally, measuring A_{zz} at lower Q^2 will map out the transition from hadronic to partonic degrees of freedom.

Ratios of inclusive cross sections at $x > 1$ has demonstrated an early onset of the scaling of the ratios when plotted as a function of the light-cone fraction of the struck nucleon momentum. As a result, the ratios provide a direct measurement of the ratio of the high momentum components in nuclei. Similarly, one can expect that in the case of scattering from the polarized deuteron we expect the early scaling for the asymmetry when plotted as a function of the minimal struck

nucleon momentum or the light cone fraction in the A(e, e') case. It was observed at JLab that the scaling of the ratios set in starting at $Q^2 \sim 1$ GeV^2 [9] so covering the range of Q^2 up to 2 GeV^2 will be sufficient to measure the S/D ratios in an interesting momentum range.

It is worth noting here that in addition to comparing predictions for the different wave functions, one expects to be able to distinguish between non-relativistic and light cone quantum mechanic models. The principal difference between the models is the relation between the spectator momentum and momentum in the wave function. In the nonrelativistic model they coincide, while in the light cone model the relation is non-linear starting at $k \sim 250$ MeV$/c$. This difference is most clearly manifested in the scattering from the polarized deuteron due to a strong dependence of the S/D ratio on the nucleon momentum.

1.2 Study of the Relativistic NN Bound System

One of the important issues in studying of nuclear structure at short distances is the relativistic description of the bound system. This is an important issue also in understanding the QCD medium effect with recent studies indicating that parton distribution modifications in nuclei are proportional to the high momentum component of nuclear wave function.

The deuteron is the simplest bound system and naturally any self-consistent attempt to understand the relativistic effects in the bound nuclear systems should start with the deuteron. The issue of the relativistic description of the deuteron has long history with extensive research that started in late 1970's [12, 13, 14, 7].

The experimental studies of the relativistic effects in the deuteron up to now include the large Q^2 elastic ed scattering [15], however due to complexities in the reaction mechanism [16] the relativistic effects were difficult to isolate.

The inclusive D(e, e')X experiments from tensor-polarized deuterons at $Q^2 > 1$ GeV^2 and $x > 1$ region gives a new possibility to probe the relativistic structure of the deuteron. In this case the use of the tensor polarized deuteron allows us to prepare the nucleus in the most compact state in which, due to the absence of the pure S-wave^2 contribution, the system in average is sensitive to the higher moment of the nucleon in the deuteron. At large $Q^2 > 1$ GeV^2 kinematics, the probed longitudinal momenta of the bound nucleon $p_z \approx m_N(1-x)$, or the light cone momentum fraction $\alpha \geq x$. Because of these kinematic conditions and the absence of the large S-wave^2 contribution, one expects a measurable relativistic effects already at $x \leq 1.2$.

The biggest advantage is that one expects less uncertainty due to the choice of the NN potential and reaction dynamics due to relatively small values of the bound nucleon momenta involved (≥ 200 MeV$/c$).

The sensitivity to relativistic effects is estimated using the theoretical calculations based on two very different approaches. The first approach treats the virtuality of the bound nucleon within a description of the deuteron in the lab. frame with treating the interacting nucleon as being virtual (virtual nucleon, or VN, approximation) by taking the residue over the energy of the spectator nucleon. In this case, the deuteron wave function satisfies the covariant equation of two-nucleon bound system with spectator being on energy shell [17, 18].

Another approach is based on the observation that high energy processes evolve along the light-cone (LC). Therefore, it is natural to describe the reaction within the light-cone non-covariant

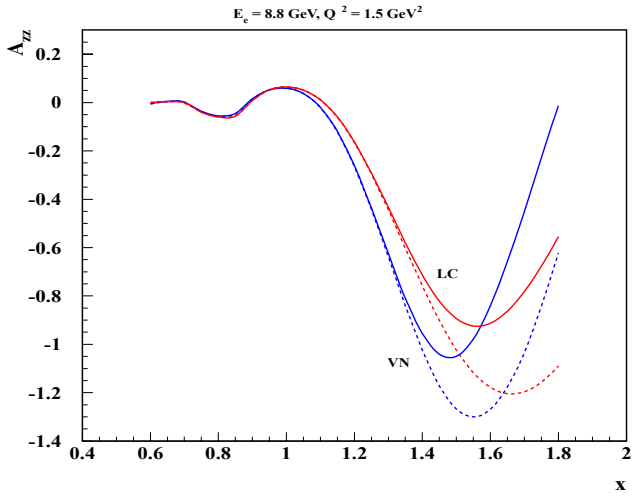

Figure 2: The A_{zz} observable calculated at $Q^2 = 1.5$ $(\mathrm{GeV}/c)^2$ using the light-cone (red) and virtual nucleon (blue) models with NN potential inputs of AV18 (solid) and CDBonn (dotted). Calculations provided by M. Sargsian and M. Strikman [19].

framework [7]. Negative energy states do not enter in this case, though one has to take into account so called instantaneous interactions. In the approximation when non-nucleonic degrees of freedom in the deuteron wave function can be neglected, one can unambiguously relate the light-cone wave functions to those calculated in the lab. frame by introducing the LC pn relative three momentum,

$$k = \sqrt{\frac{m^2 + p_t^2}{\alpha(2-\alpha)} - m^2}. \tag{2}$$

In Fig. 2, the prediction for VN [17] and LC [8] approximations are given for the highest Q^2 kinematics proposed. As was previously mentioned, a measurable difference is predicted to be observable already at $x \geq 1.2$. to the choice of the wave function.

1.3 Interest from Theorists

The measurement proposed in this letter has stirred interest in a number of theorists who are working on calculations. Many of these are on-going and are expected to be completed in the coming months to further the physics motivation of a measurement of A_{zz} in the quasi-elastic region at various momentum-transfer.

The light cone and virtual nucleon calculations of M. Sargsian [20] and M. Strikman [21] are already available for A_{zz} and are presented in this document. Early calculations of the M. Strikman light-cone model indicate a potential measurable discrepancy based on the input of different NN potentials, but the results are very preliminary and require further investigation. S. Liuti has agreed to join in this theoretical effort, stating "This is an important measurement to know, and should be calculated more thoroughly." [22]

Models involving 6-quark calculations of quasi-elastic A_{zz} can be calculated by G. Miller [23] and have been motivated by the collaboration. In his own words, he states "This measurement was a highlighted need early at JLab. A new measurement at higher Q^2 would be very interesting. In principle such could test my model. I could calculate the influence of my 6-quark configurations on elastic scattering."

Continuing his interest from DIS b_1 calculations, W. Cosyn is developing calculations of the quasi-elastic contribution to inclusive deuteron scattering, which will be the dominant contribution in the $x > 1$ regime [24]. His calculations, which include final-state interactions, can be modified to include A_{zz} and expects to have them within the coming months. In his words, "I hope to do some calculations soon and could easily do them for the kinematics in your proposal."

In addition, W. Van Orden has calculations in progress using different nucleon-nucleon potentials, as well as different prescriptions for handling the reactions mechanisms [5]. Similar calculations are currently being finalized for the approved D$(e, e'p)n$ at high Q^2, high p_m experiment. Once completed, he will turn his attention to tensor polarization observables in the low Q^2 region and investigate the effects from differing NN potentials.

In summary, we are encouraged that several theorists have begun serious efforts to calculate A_{zz} in the $x > 1$ region using a variety of models. We anticipate that the PAC's guidance will further encourage and focus these efforts.

2 T_{20} Background

For the following discussion we use the nomenclature described by the Madison Convention [25].

3 The Proposed Experiment

We propose to measure the tensor asymmetry A_{zz} and tensor analyzing power T_{20} from inclusive electron scattering from polarized deuterons in the quasi-elastic and elastic region of $0.30 < x < 2.0$, 0.2 (GeV/c)^2 $< Q^2 < 2.9$ (GeV/c)^2, and $1.8 < W < 3.1$ GeV using the Hall C HMS and SHMS spectrometers at forward angle using a solid polarized ND_3 target.

3.1 A_{zz} Experimental Method

The measured double differential cross section for a spin-1 target is characterized by a vector polarization P_z and tensor polarization P_{zz} is expressed as,

$$\frac{d^2\sigma_p}{d\Omega dE'} = \frac{d^2\sigma_u}{d\Omega dE'}\left(1 - P_z P_B A_1 + \frac{1}{2}P_{zz}A_{zz}\right), \tag{3}$$

where, σ_p (σ_u) is the polarized (unpolarized) cross section, P_B is the incident electron beam polarization, and A_1 (A_{zz}) is the vector (tensor) asymmetry of the virtual-photon deuteron cross section. This allows us to write the polarized tensor asymmetry with positive tensor polarization using an

unpolarized electron beam as

$$A_{zz} = \frac{2}{P_{zz}} \left(\frac{\sigma_p - \sigma_u}{\sigma_u} \right). \tag{4}$$

The tensor polarization is given by

$$P_{zz} = \frac{n_+ - 2n_0 + n_-}{n_+ + n_- + n_0}, \tag{5}$$

where n_m represents the population in the $m_z = +1$, -1, or 0 state.

Eq. 4 reveals that the asymmetry A_{zz} compares two different cross sections measured under different polarization conditions of the target: positively tensor polarized and unpolarized. To obtain the relative cross section measurement in the same configuration, the same target cup and material will be used at alternating polarization states (polarized vs. unpolarized), and the magnetic field providing the quantization axis will be oriented along the beamline at all times. This field will always be held at the same value, regardless of the target material polarization state. This process, identical to that used for the E12-13-011 b_1 measurement, ensures that the acceptance remains consistent within the stability (10^{-4}) of the super conducting magnet.

Since many of the factors involved in the cross sections cancel in the ratio, Eq. 4 can be expressed in terms of the charge normalized, efficiency corrected numbers of tensor polarized (N_p) and unpolarized (N_u) counts,

$$A_{zz} \;=\; \frac{2}{f P_{zz}} \left(\frac{N_p - N_u}{N_u} \right). \tag{6}$$

The dilution factor f corrects for the presence of unpolarized nuclei in the target and is defined by

$$f = \frac{N_D \sigma_D}{N_N \sigma_N + N_D \sigma_D + \sum\limits_A N_A \sigma_A}, \tag{7}$$

where N_D is the number of deuterium nuclei in the target and σ_D is the corresponding inclusive double differential scattering cross section, N_N is the nitrogen number of scattered nuclei with cross section σ_N, and N_A is the number of other scattering nuclei of mass number A with cross section σ_A. As has been noted in previous work [1], the dilution factor at high x drops off considerably until the SRC plateau region, as shown in Fig. 3. By using a high-luminosity solid target and a low scattering angle $\theta_{e'}$, this effect will be counteracted. The dilution factor is a much smaller problem for elastic scattering at $x = 2$.

The dilution factor can be written in terms of the relative volume ratio of ND_3 to LHe in the target cell, otherwise known as the packing fraction p_f. In our case of a cylindrical target cell oriented along the magnetic field,the packing fraction is exactly equivalent to the percentage of the cell length filled with ND_3.

If the time is evenly split between scattering off of polarized and unpolarized ND_3, the time necessary to achieve the desired precision δA is:

$$T = \frac{N_p}{R_p} + \frac{N_u}{R_u} = \frac{8}{f^2 P_{zz}^2} \left(\frac{R_p (R_u + R_p)}{R_u^3} \right) \frac{1}{\delta A_{zz}^2} \tag{8}$$

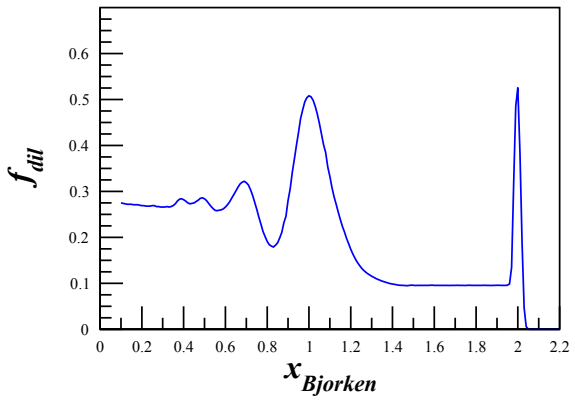

Figure 3: The estimated dilution factor, in this case at $Q^2 = 1.5\ (\mathrm{GeV}/c)^2$, is expected to drop off at high x until it reaches the SRC plateau region and then the elastic peak at $x = 2$. The low dilution factor of $1.1 < x < 1.95$ will be counteracted by using a high-luminosity target.

where $R_{p(u)}$ is the polarized (unpolarized) rate and $N_{p(u)}$ is the total estimated number of polarized (unpolarized) counts to achieve the uncertainty δA_{zz}.

3.2 T_{20} Experimental Method

A measurement of T_{20} will be extracted from A_{zz} on the elastic peak for each Q^2 mentioned in Section 3.5. We will follow a similar method to B. Boden *et al* [26], which also measured T_{20} using a tensor polarized target. Our methods differ only in that we will use the high resolution of the HMS and SHMS to determine the elastic peak through kinematic cuts, where Boden utilized a second spectrometer for that purpose.

Boden describes the relationship between the measured ratio of unpolarized and tensor-polarized yields and T_{20} in the following manner. They start with the experimental ratio R_{exp} between the tensor polarized and unpolarized states,

$$R_{exp} = \frac{d\sigma_p}{d\sigma_u} = 1 + P_{zz}\left(\frac{d\sigma_T - d\sigma_u}{d\sigma_u}\right) = 1 + P_{zz}\left(R_T - 1\right) \tag{9}$$

$$R_T - 1 = \frac{1}{P_{zz}}\left(\frac{d\sigma_p}{d\sigma_u} - 1\right). \tag{10}$$

This matches closely to our definition of A_{zz},

$$A_{zz} = \frac{2}{f P_{zz}}\left(\frac{d\sigma_p}{d\sigma_u} - 1\right), \tag{11}$$

where the dilution factor would be $f = 1$ in the Boden extraction, since they are tagging deuterons and have negligible contamination from other sources.

Thus, R_T and A_{zz} are related by

$$R_T - 1 = \frac{1}{2} A_{zz}. \tag{12}$$

Utilizing forward electron scattering to reduce magnetic contributions to a negligible amount, $(R_T - 1)$ is related to T_{20} by

$$T_{20} = -\sqrt{8}(R_T - 1), \tag{13}$$

which we can use to relate T_{20} to an elastic measurement of A_{zz} by

$$T_{20} = -\sqrt{2} A_{zz}. \tag{14}$$

3.3 Polarized Target

This experiment will use the JLab/UVa dynamically polarized solid ND_3 target operated in longitudinal mode. The target is typically operated with a specialized slow raster and beamline instrumentation capable of characterizing the low current 50-100 nA beam. All of these requirements have been met previously in Hall C. The polarized target (see Fig. 4), has been successfully used in experiments E143, E155, and E155x at SLAC, and E93-026, E01-006 and E07-003, E08-027 and E08-007 at JLab. A similar target was used in Hall B for the EG1, EG4, and DVCS experiments.

The JLab/UVa target underwent significant renovation and improvement [27] during the recent g2p run. The magnet was replaced early in the run, and the target then performed consistently. A new 1 K refrigerator and target insert were designed and constructed by the JLab target group. The cryogenic pumping system has been overhauled. In particular, the older Alcatel 2060H rotary vane pumps have been replaced with new Pfeiffer DU065 magnetically coupled rotary vane pumps, and the pump controls are being refurbished. The target motion system has been rebuilt from scratch.

The target operates on the principle of Dynamic Nuclear Polarization, to enhance the low temperature (1 K), high magnetic field (5 T) polarization of solid materials by microwave pumping. The polarized target assembly contains several target cells of 3.0 cm length that can be selected individually by remote control to be located in the uniform field region of a superconducting Helmholtz pair. The permeable target cells are immersed in a vessel filled with liquid Helium and maintained at 1 K by use of a high power evaporation refrigerator. The coils have a 50° conical shaped aperture along the beam axis which allow for unobstructed forward scattering.

The target material is exposed to microwaves to drive the hyperfine transition which aligns the nucleon spins. The heating of the target by the beam causes a drop of a few percent in the polarization, and the polarization slowly decreases with time due to radiation damage. Most of the radiation damage can be repaired by periodically annealing the target, until the accumulated dose reached is greater than about 0.5×10^{17} e^-/cm^2, at which time the target material needs to be replaced.

3.3.1 Polarization Analysis

The three Zeeman sublevels of the deuteron system ($m = -1, 0, 1$) are shifted unevenly due to the quadrupole interaction [28]. This shift depends on the angle between the magnetic field and

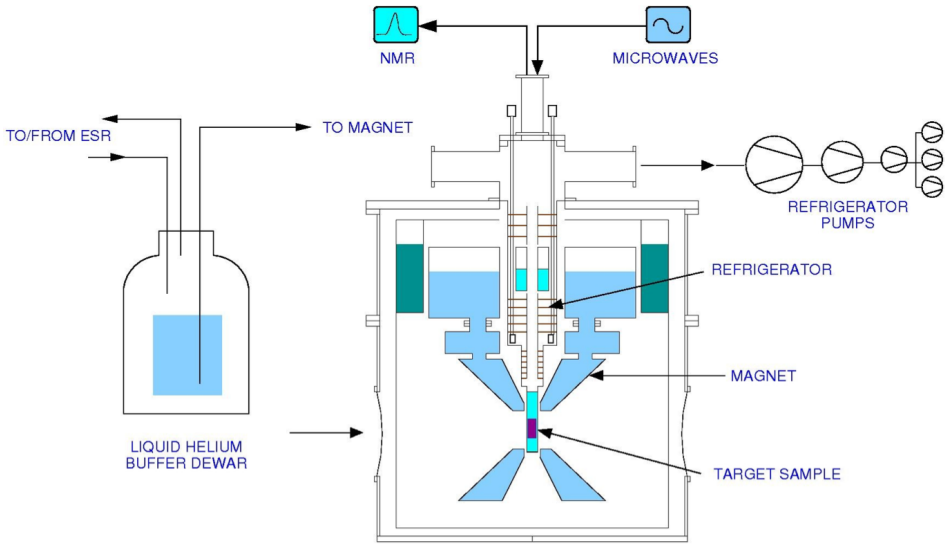

Figure 4: Cross section view of the JLab/UVa polarized target. The proposed experiment will use the modified Hall B magnet, where the backwards-scattering cone is blocked with quench protection circuitry. Figure courtesy of C. Keith.

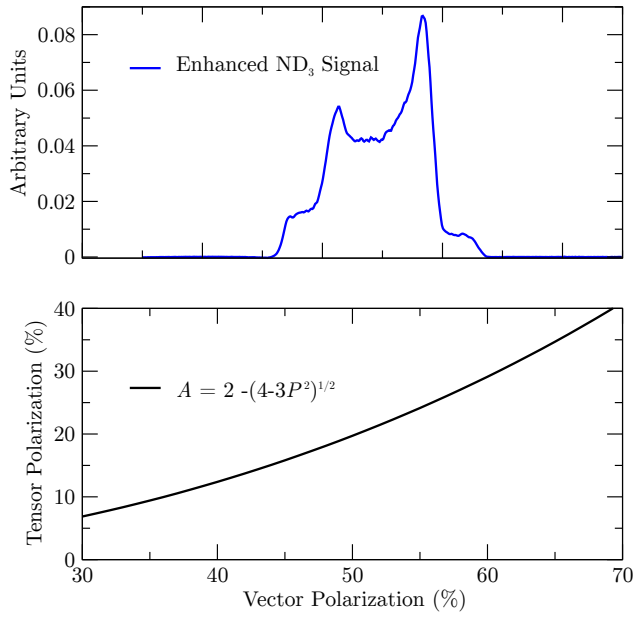

Figure 5: **Top**: NMR signal for ND_3 with a vector polarization of approximately 50% from the GEN experiment. **Bottom**: Relationship between vector and tensor polarization in equilibrium, and neglecting the small quadrupole interaction.

the electrical field gradient, and gives rise to two separate transition energies. Hence, the unique double peaked response displayed in Fig. 5. When the system is at thermal equilibrium with the solid lattice, the deuteron polarization is known from:

$$P_z = \frac{4 + \tanh \frac{\mu B}{2kT}}{3 + \tanh^2 \frac{\mu B}{2kT}} \tag{15}$$

where μ is the magnetic moment, and k is Boltzmann's constant. The vector polarization can be determined by comparing the enhanced signal with that of the TE signal (which has known polarization). This polarimetry method is typically reliable to about 3.9% relative.

Similarly, the tensor polarization is given by:

$$P_{zz} = \frac{4 + \tanh^2 \frac{\mu B}{2kT}}{3 + \tanh^2 \frac{\mu B}{2kT}} \tag{16}$$

From Eqs. 15 and 16, we find:

$$P_{zz} = 2 - \sqrt{4 - 3P_z^2}$$

In addition to the TE method, polarizations can be determined by analyzing NMR lineshapes as described in [29] with a typical 7% relative uncertainty. At high polarizations, the intensities of the two transitions differ, and the NMR signal shows an asymmetry R in the value of the two peaks, as shown in Fig. 5. The vector polarization is then given by:

$$P_z = \frac{R^2 - 1}{R^2 + R + 1} \tag{17}$$

and the tensor polarization is given by:

$$P_{zz} = \frac{R^2 - 2R + 1}{R^2 + R + 1} \tag{18}$$

This measuring technique can be used as a compliment to the TE method resulting in reduced uncertainty in polarization.

3.3.2 Tensor Polarization Enhancement

It is possible to enhance tensor polarization using RF irradiation on the oriented deuterium nuclei to manipulate the alignment. Applying a saturating RF field on the pedestal of the smaller transition equalizes the substate $m = +1$ and $m = 0$ populations over 2/3 of the NMR signal. This equalization over the range of a single pedestal leads to enhancement in tensor polarization with only a small loss to the overall area ($\sim 2\%$). Very recent studies at UVA using deuterated butanol have indicated that the tensor polarization can be increased by using a modified hole burning technique. The result will be investigated in the near future, and the method applied to ND_3. The studies also indicate that microwaves used during DNP does not interfere with the saturation from the RF irradiation when sufficient power is used. This implies that RF over the pedestal can be done the same time DNP is performed to enhance the area while taking beam in an experiment. Research and development is ongoing to study various techniques to optimize tensor enhancement for nuclear experiments targets.

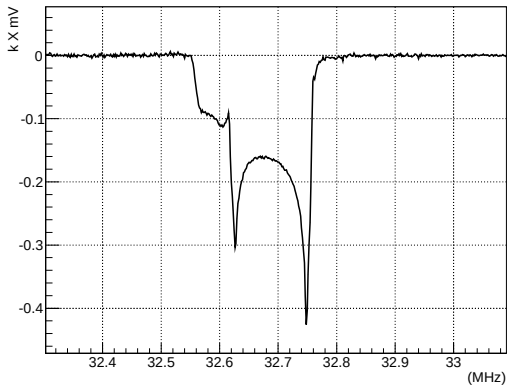

Figure 6: The deuterium magnetic resonance line shape showing the recent achievement of high tensor polarization of deuterated butanol after RF saturation of a pedestal at the UVA polarized target lab accomplished during their April 2014 cool-down.

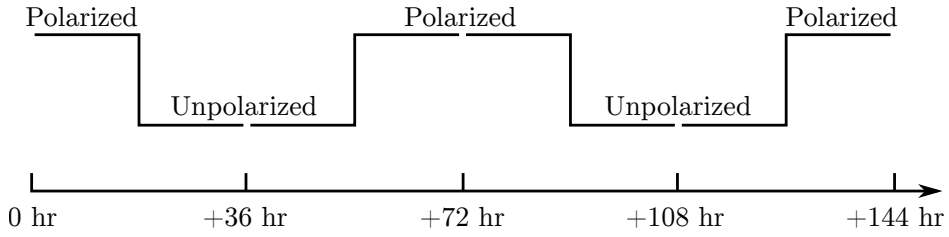

Figure 7: A visual demonstration of how the polarization cycle will happen over a 72 hour period to reduce time-dependent systematic effects. For the two lower Q^2 measurements, the cycle will happen over a 18 hour period.

3.3.3 Depolarizing the Target

To move from polarized to unpolarized measurements, the target polarization will be annihilated using destructive NMR loop field changes and destructive DNP microwave pumping. During unpolarized data taking the incident electron beam heating is enough to remove the thermal equilibrium polarization.

We are able to verify that the target is in the unpolarized state via NMR measurements. The target material will be kept at 1 K for polarized and unpolarized data collection, and the target field will be held constant for both states as well. These consistencies are used to minimize the systematic differences in the polarized and unpolarized data collection. To minimize systematic effects over time, the polarization condition will be switched twice in a 72 hour period, as shown in Fig. 7. This will be sufficient to account for drift in integrated charge accumulation.

3.3.4 Dilution Factor

To derive the dilution factor, we first start with the ratio of polarized to unpolarized counts. In each case, the number of counts that are actually measured, neglecting the small contributions of the thin aluminium cup window materials, NMR coils, etc., are

$$N_1 = Q_1 \varepsilon_1 \mathcal{A}_1 l_1 [(\sigma_N + 3\sigma_1) p_f + \sigma_{He}(1 - p_f)], \tag{19}$$

and

$$N = Q \varepsilon \mathcal{A} l [(\sigma_N + 3\sigma) p_f + \sigma_{He}(1 - p_f)]. \tag{20}$$

where Q represents accumulated charge, ε is the dectector efficiency, $\mathcal{A}$ the cup acceptance, and l the cup length.

For this calculation we assume similar charge accumulation such that $Q \simeq Q_1$, and that the efficiencies stay constant, in which case all factors drop out of the ratio leading to

$$\begin{aligned}
\frac{N_1}{N} &= \frac{(\sigma_N + 3\sigma_1) p_f + \sigma_{He}(1 - p_f)}{(\sigma_N + 3\sigma) p_f + \sigma_{He}(1 - p_f)} \\
&= \frac{(\sigma_N + 3\sigma(1 + A_{zz} P_{zz}/2)) p_f + \sigma_{He}(1 - p_f)}{(\sigma_N + 3\sigma) p_f + \sigma_{He}(1 - p_f)} \\
&= \frac{[(\sigma_N + 3\sigma) p_f + \sigma_{He}(1 - p_f)] + 3\sigma A_{zz} P_{zz}/2}{(\sigma_N + 3\sigma) p_f + \sigma_{He}(1 - p_f)} \\
&= 1 + \frac{3\sigma A_{zz} P_{zz}/2}{(\sigma_N + 3\sigma) p_f + \sigma_{He}(1 - p_f)} \\
&= 1 + \frac{1}{2} f A_{zz} P_{zz},
\end{aligned} \tag{21}$$

where $\sigma_1 = \sigma(1 + A_{zz} P_{zz}/2)$ has ben substituted, per Eq. 3, with $P_B = 0$. It can be seen that the above result corresponds to Eq. 6.

3.4 Overhead

Table 1 summarizes the expected overhead, which sums to 10.3 days. The dominant overhead comes from switching from the polarized to unpolarized state and vice versa, and target anneals. The target will need to be annealed about every other day, and the material replaced once a week. Measurements of the dilution from the unpolarized materials contained in the target, and of the packing fraction due to the granular composition of the target material will be performed with a carbon target.

3.5 Kinematics

We propose to measure the tensor asymmetry A_{zz} for $0.30 < x < 2.0$, 0.2 (GeV/c)^2 $< Q^2 <$ 2.9 (GeV/c)^2, and $1.8 < W_{NN} < 3.1$ GeV and extract the tensor analyzing power T_{20} for 0.2 (GeV/c)^2 $< Q^2 < 1.5$ (GeV/c)^2. Central kinematics of the spectrometers are given in Table 2 .

Overhead	Number	Time Per (hr)	(hr)
Polarization/depolarization	38	2.0	76.0
Target anneal	15	4.0	60.0
Target T.E. measurement	6	4.0	24.0
Target material change	4	4.0	16.0
Packing Fraction/Dilution runs	20	1.0	20.0
BCM calibration	9	2.0	18.0
Optics	3	4.0	12.0
Linac change	2	8.0	16.0
Momentum/angle change	3	2.0	6.0
			10.3 days

Table 1: Major contributions to the overhead.

	E_0 (GeV)	Q^2 (GeV^2)	E' (GeV)	$\theta_{e'}$ ($^\circ$)	Rates (kHz)	PAC Time (Days)
SHMS (S1)	8.8	1.5	8.36	8.2	0.38	25
HMS (H1)	8.8	2.9	7.26	12.2	0.04	25
SHMS (S2)	6.6	0.7	6.35	7.5	3.57	8
HMS (H2)	6.6	1.8	5.96	12.3	0.09	8
SHMS (S3)	2.2	0.2	2.15	10.9	10.5	1
HMS (H3)	2.2	0.3	2.11	14.9	3.23	1

Table 2: Summary of the central kinematics and physics rates using the Hall C spectrometers.

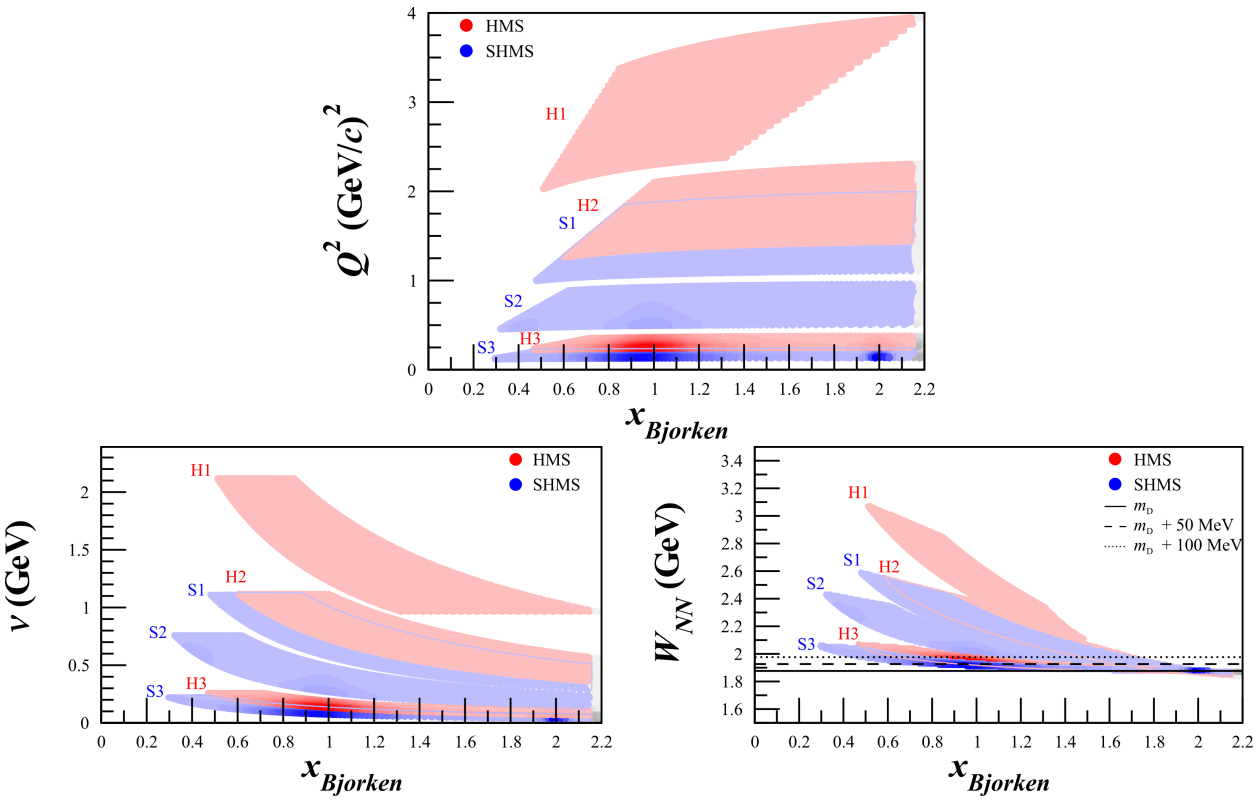

Figure 8: Kinematic coverage for central spectrometer settings at $Q^2 = 2.9$ $(\mathrm{GeV}/c)^2$ (H1), 1.8 $(\mathrm{GeV}/c)^2$ (H2), 1.5 $(\mathrm{GeV}/c)^2$ (S1), 0.7 $(\mathrm{GeV}/c)^2$ (S2), 0.3 $(\mathrm{GeV}/c)^2$ (H3), and 0.2 $(\mathrm{GeV}/c)^2$ (S3). The grey regions are not included in our statistics estimates since they fall outside the range of electron-deuteron scattering. Darker shading represents areas with higher statistics. The solid, dashed, and dotted lines in the W_{NN} plot indicate deuteron mass, deuteron mass + 50 MeV, and deuteron mass + 100 MeV, respectively.

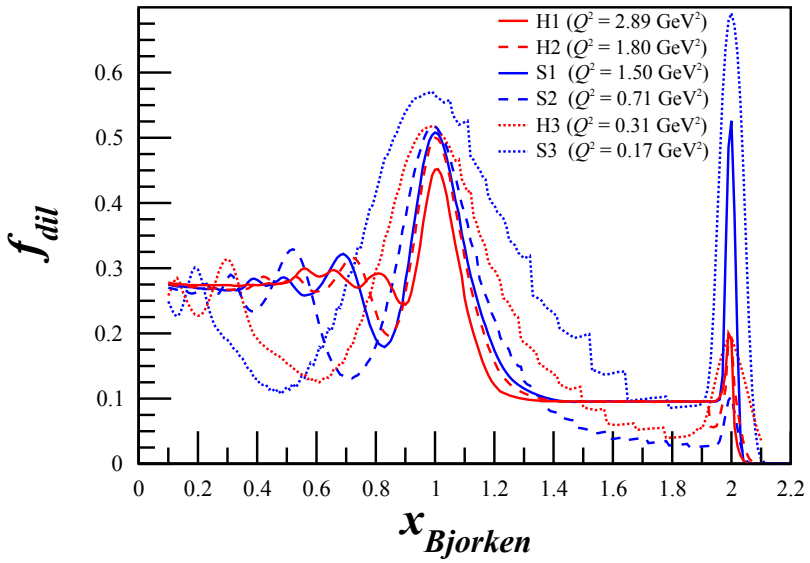

Figure 9: Projected dilution factor covering the entire x range to be measured using a combination of P. Bosted's [30] and M. Sargsian's [20] code, along with a calculation of the elastic peak using a parametrization of the deuteron form factors, for the SHMS and HMS.

Fig. 8 shows the planned kinematic coverage utilizing the Hall C HMS and SHMS spectrometers at forward angles.

The polarized ND_3 target is discussed in Section 3.3. The magnetic field of the target will be held constant along the beamline at all times, while the target state is alternated between a polarized and unpolarized state. The tensor polarization and packing fraction used in the rates estimate are 30% and 0.65, respectively. The dilution factor in the range of this measurement is shown in Fig. 9. The spread of the elastic peak for the dilution factor was calculated assuming a momentum resolution of 0.1% for the HMS and 0.08% for the SHMS. With an incident electron beam current of 80 nA, the expected deuteron luminosity is 1.2×10^{35} cm^{-2}s^{-1}.

The momentum bite and the acceptance were assumed to be $\Delta P = \pm 8\%$ and $\Delta\Omega = 5.6$ msr for the HMS, and $\Delta P = ^{+20\%}_{-8\%}$ and $\Delta\Omega = 4.4$ msr for the SHMS. For the choice of the kinematics, special attention was taken onto the angular and momentum limits of the spectrometers with a longitudinal polarized target: for the HMS, $12.2^\circ \leq \theta \leq 85^\circ$ and $1 \leq P_0 \leq 7.3$ GeV/c, and for the SHMS, $5.5^\circ \leq \theta \leq 40^\circ$ and $2 \leq P_0 \leq 11$ GeV/c. In addition, the opening angle between the spectrometers is physically constrained to be larger than 17.5°.

A total of 34 days of beam time is requested for production data, with an additional 10.3 days of expected overhead.

Source	Systematic
P_{zz} Polarimetry	12%
Dilution Factor	6.0%
Packing Fraction	3.0%
Trigger/Tracking Efficiency	1.0%
Acceptance	0.5%
Charge Determination	1.0%
Detector Resolution and Efficiency	1.0%
Total	14%

Table 3: Estimates of the scale dependent contributions to the systematic error of A_{zz}.

3.6 Uncertainty Estimates

We discuss here the expected statistical and systematic uncertainties that we expect to contribute to the measurement.

3.6.1 Systematic Uncertainty

Table 3 shows a list of the scale dependent uncertainties contributing to the systematic error in A_{zz}. With careful uncertainty minimization in polarization the relative error in vector polarization, Pz, can be less than or equal to 3.9%, as was demonstrated for the proton in the recent E08-027/E08-007 experiment [31] and nearly as good for the deuteron using multiple techniques to measure the NMR signal as discussed in [32]. With the use of a positive tensor enhanced target it has been projected to be able to achieve a relative error in P_{zz} better than 12% [32]. The uncertainty from the dilution in the polarized target is estimated to be about 6% over the range of kinematics points of interest. We consider separately the uncertainty in the packing fraction of the ammonia target contributes at a level of less than 3%. Charge calibration and detector efficiencies are expected to be known better to 1%.

Time Dependent Systematic Effects

Eq. 6 involves the ratio of counts, which leads to cancellation of several first order systematic effects. However, the fact that the two data sets will not be taken simultaneously leads to a sensitivity to time dependent variations which will be monitored and suppressed. The typical size of these types of effects are small compared to the large asymmetries predicted for most of the proposed kinematic regions, but must be carefully monitored whenever the expected asymmetry is small, such as at a zero crossing.

To investigate the systematic differences in the time dependent components of the integrated counts, we need to consider the effects from calibration, efficiency, acceptance, and luminosity between the two polarization states.

Fluctuations in luminosity due to target density variation can easily be kept to a minimum by

keeping the material beads at the same temperature for both polarization states by control of the microwave and the LHe evaporation. The He vapor pressure reading gives accuracy of material temperature changes at the level of $\pm 0.1\%$.

The beam charge asymmetries between two helicity states using the luminosity monitors for experiment E06-010 has been shown to be at the level of 4×10^{-5} with a width of 2×10^{-4}. An additional estimate on the change in the BCM calibration constant is seen in experiment E08-027 resulting in a absolute deviation of 2×10^{-4} over the course of six days. We expect to be able to minimize long term drifts by careful thermal isolation of the BCMs.

The acceptance of each cup can only change as a function of time if the magnetic field changes. The capacity to set, reset, and hold the target superconducting magnet to a desired holding field causes a field uncertainty of $\delta B/B = 0.01\%$. This implies that, like the cup length l, the acceptance $\mathcal{A}$ for each polarization state is the same.

In order to look at the effect on A_{zz} due to drifts in beam current monitor calibration and detector efficiency, we rewrite Eq. 6 explicitly in terms of the raw measured counts N_p^c and N_u^c,

$$\begin{aligned} A_{zz} &= \frac{2}{fP_{zz}} \left(\frac{N_p^c}{N_u^c} - 1 \right) \\ &= \frac{2}{fP_{zz}} \left(\frac{Q\varepsilon l\mathcal{A}}{Q_1\varepsilon_1 l\mathcal{A}} \frac{N_p}{N_u} - 1 \right) \end{aligned} \tag{22}$$

where Q represents the accumulated charge, and ε is the detector efficiency. The target length l and acceptance $\mathcal{A}$ are identical in both states to first order.

We can then express Q_1 as the change in beam current measurement calibration that occurs in the time it takes to collect data in one polarization state before switching to another, such that $Q_1 = Q(1 - dQ)$. In this notation, dQ is a dimensionless ratio of changes in different polarization states and would ideally be equal to zero. A similar representation is used for drifts in detector efficiency leading to,

$$A_{zz} = \frac{2}{fP_{zz}} \left(\frac{N_p Q(1 - dQ)\varepsilon(1 - d\varepsilon)}{N_u Q\varepsilon} - 1 \right). \tag{23}$$

which simplifies to,

$$A_{zz} = \frac{2}{fP_{zz}} \left(\frac{N_p}{N_u}(1 - dQ - d\varepsilon + dQd\varepsilon) - 1 \right). \tag{24}$$

We obtain estimates of dQ and $d\varepsilon$ from previous experimental studies. During the JLab transversity experiment E06-010, the detector drift was measured such that the normalized yield over a three month period indicated little change ($< 1\%$). These measurement were then used to show that for short time (20 minutes periods between target spin flip), the detector drift was estimated to be less than 1% times the ratio of the time period between target spin flip and three months. For the present experiment we use the same estimate except for the period between target polarization states used is ≈ 36 hours leading to an overall drift $d\varepsilon \approx 0.01\%$. A similar approach is used to establish an estimate for dQ using studies from the data from the E08-027 experiment resulting in $d\varepsilon \approx 0.01\%$.

To express A_{zz} in terms of the estimated experimental drifts in efficiency and current measurement we can write,

$$A_{zz} = \frac{2}{fP_{zz}}\left(\frac{N_1}{N} - 1\right) \pm \frac{2}{fP_{zz}} d\xi. \tag{25}$$

This leads to a contribution to A_{zz} on the order of 1×10^{-3},

$$dA_{zz}^{drift} = \pm\frac{2}{fP_{zz}} d\xi = \pm 3.7 \times 10^{-3}. \tag{26}$$

Naturally detector efficiency can drift for a variety of reasons, for example including fluctuations in gas quality, HV drift or drifts in the spectrometers magnetic field. All of these types of variation as can be realized both during the experiment though monitoring as well as systematic studies of the data collected. Checks on the consistency of the cross section data that can be use ensuring the quality of each run will be used in the asymmetry analysis. Regression can be use to correct for any long term drifts that are of a non-stochastic nature. Each of these systematic effects can mitigate the systematic uncertainty to ~ 0.001. In the kinematic region proposed here, A_{zz} is expected to be large, on the order of 0.1 to 1.0, making any absolute errors on this scale only critical as the data and models pass through the x-axis.

3.6.2 Statistical Uncertainty

To investigate the statistical uncertainty we start with the equation for A_{zz} using measured counts for polarized data (N_p) and unpolarized data (N_u),

$$A_{zz} = \frac{2}{fP_{zz}}\left(\frac{N_p}{N_u} - 1\right). \tag{27}$$

The statistical error with respect to counts is then

$$\delta A_{zz} = \frac{2}{fP_{zz}}\sqrt{\left(\frac{\delta N_p}{N_u}\right)^2 + \left(\frac{N_p \delta N_u}{N_u^2}\right)^2}. \tag{28}$$

For $\delta N_{p(u)} = \sqrt{N_{p(u)}}$, the uncertainty becomes

$$\delta A_{zz} = \frac{2}{fP_{zz}}\sqrt{\frac{N_p(N_u + N_p)}{N_u^3}}, \tag{29}$$

which can't be simplified further due to the large expected asymmetry.

The number of counts was calculated using a combination of P. Bosted's [30] and M. Sargsian's [20] code for $x < 2$. The Bosted code was used for the lowest Q^2 setting, where effects of SRC scaling are expected to be negligible, and for $x < 1.1$ to accurately determine the quasi-elastic peak. The Sargsian code was used for the higher Q^2 settings at $x > 1.1$ due to its inclusion of SRC scaling effects.

The deuteron elastic peak was calculated using a parametrization of the deuteron elastic form factors A and B by

$$\frac{d^2\sigma}{d\Omega dE'} = \sigma_{\text{Mott}} \left(\frac{E'}{E}\right) \left[A + B\tan^2\left(\frac{\theta}{2}\right)\right] \delta(E' - E'_{el}), \tag{30}$$

where $\delta(E' - E'_{el})$ is approximated by a Gaussian distribution with its width determined by the resolution of the spectrometers,

$$\delta(E' - E'_{el}) = \frac{1}{2\Delta E \cdot E'_{el}\sqrt{\pi}} e^{-\frac{(E'-E'_{el})^2}{2(\Delta E \cdot E'_{el})^2}}, \tag{31}$$

where $\Delta E = 0.1\ (0.08)\%$ for the HMS (SHMS) and $E'_{el} = \frac{Q^2}{2m_D}$. This was added to the rates calculation that was used for quasi-elastic A_{zz} and b_1 [33]. The uncertainty of A_{zz} on the elastic peak was calculated the same as Eq. 29.

Following the methodology discussed in Section 3.2, to obtain statistical uncertainties for T_{20} we scale our calculated elastic A_{zz} uncertainties by

$$\delta t_{20} = \sqrt{2}\delta A_{zz}. \tag{32}$$

The projected uncertainties for A_{zz} are summarized in Tables 4-5 and displayed in Figs. 10-11. The projected uncertainties for T_{20} are summarized in Table 6 [citation needed]and displayed in Fig. 12.

4 PAC42 Comments and Concerns

In this section we summarize the comments and concerns that were raised by the PAC42 committees on letter of intent LOI12-14-002.

4.1 Theory Advisory Committee

> "This Letter of Intent describes a measurement of the tensor-polarized asymmetry A_{zz} in electron scattering on polarized deuterium in the quasi-elastic region, at values of $x = 0.8 - 1.75$ (x is the equivalent Bjorken variable at the nucleon level) and $Q^2 = 12\ \text{GeV}^2$. The aim is to determine with this observable the S/D wave ratio in the deuteron wave function at large relative momenta $k > 300$ MeV, which is important for understanding the NN interaction at short distances and the properties of the dominant pn short-range correlations in heavier nuclei. The same tensor-polarized asymmetry was/will be measured in elastic scattering (deuteron form factor) and deep-inelastic scattering (structure function b_1); the proposed measurement in quasi-elastic scattering would fill the gap and study this observable in the region where it is most directly related to the short-range NN interaction. The tensor asymmetry at large recoil momenta also serves as a sensitive test of "relativistic effects" in the treatment of deuteron structure, which are an important aspect of the overall theoretical framework

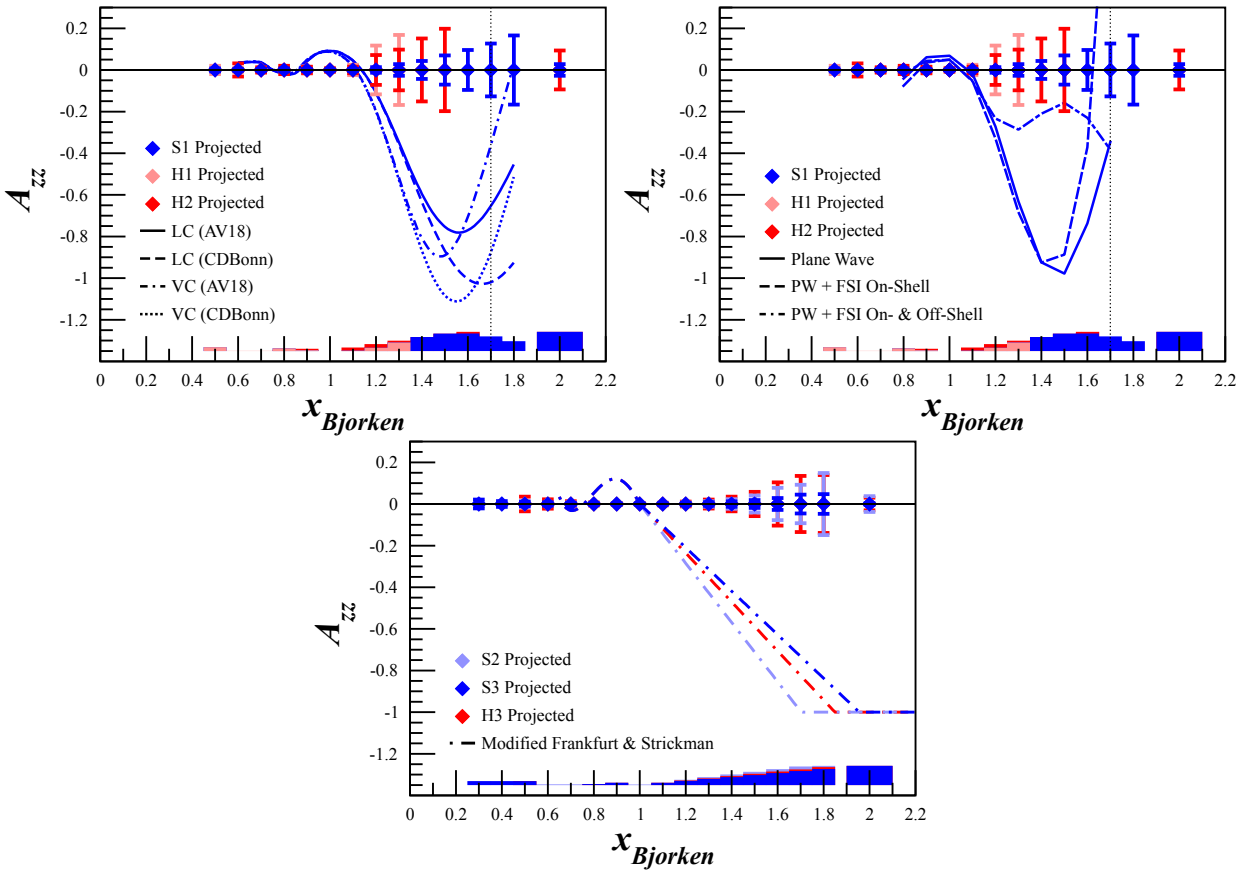

Figure 10: Projected uncertainties for the tensor asymmetry A_{zz} with 34 days of beam time. The band represents the systematic uncertainty. The top row shows the $Q^2 > 1.0$ $(\mathrm{GeV}/c)^2$ settings and the bottom row shows the $Q^2 < 1.0$ $(\mathrm{GeV}/c)^2$. The upper x limit for H1 (H2) is $x = 1.3$ ($x = 1.5$). The upper-left plot includes light-cone (LC) and virtual-nucleon (VN) calculations provided by M. Sargsian [19], as well as the dependence of each model on various deuteron wave functions (AV18, CDBonn). The dotted line at $x = 1.75$ indicates the threshold where LC and VN calculations begin to break down as A_{zz} approaches the elastic peak. The upper-right plot includes virtual-nucleon plane wave and final state interaction (FSI) calculations provided by W. Cosyn [24]. The bottom row includes a modified Frankfurt and Strikman model [1] that estimates the peak shifts in x expected due to the SRC scaling changing with Q^2 [34].

	H1: $Q^2 = 2.9$ (GeV/c)^2			H2: $Q^2 = 1.8$ (GeV/c)^2			S1: $Q^2 = 1.5$ (GeV/c)^2		
x	f_{dil}	δA_{zz}^{stat} $\times 10^{-2}$	δA_{zz}^{sys} $\times 10^{-2}$	f_{dil}	δA_{zz}^{stat} $\times 10^{-2}$	δA_{zz}^{sys} $\times 10^{-2}$	f_{dil}	δA_{zz}^{stat} $\times 10^{-2}$	δA_{zz}^{sys} $\times 10^{-2}$
0.50	0.29	2.02	1.84	—	—	—	0.25	0.72	1.84
0.60	0.29	0.91	????	0.27	3.15	????	0.30	0.36	????
0.70	0.27	1.01	????	0.32	1.26	????	0.29	0.38	????
0.80	0.30	1.11	1.34	0.20	2.00	0.48	0.17	0.74	1.34
0.90	0.24	1.73	0.38	0.27	1.45	1.10	0.29	0.44	0.38
1.00	0.46	1.03	????	0.50	0.74	????	0.51	0.24	????
1.10	0.28	2.48	0.14	0.33	1.58	1.65	0.34	0.49	0.14
1.20	0.09	11.7	1.55	0.10	7.18	3.31	0.17	1.34	1.55
1.30	0.11	16.8	4.13	0.11	9.76	4.96	0.12	2.79	4.13
1.40	—	—	—	0.12	15.1	6.65	0.13	4.30	6.72
1.50	—	—	—	0.11	19.8	8.29	0.10	7.01	8.34
1.60	—	—	—	—	—	—	0.10	9.60	8.42
1.70	—	—	—	—	—	—	0.10	12.7	7.04
1.80	—	—	—	—	—	—	0.10	16.6	4.72
2.00	—	—	—	0.20	9.33	9.20	0.50	2.79	9.20

Table 4: Summary of the expected uncertainty for each x bin for settings S1, H1, and H2.

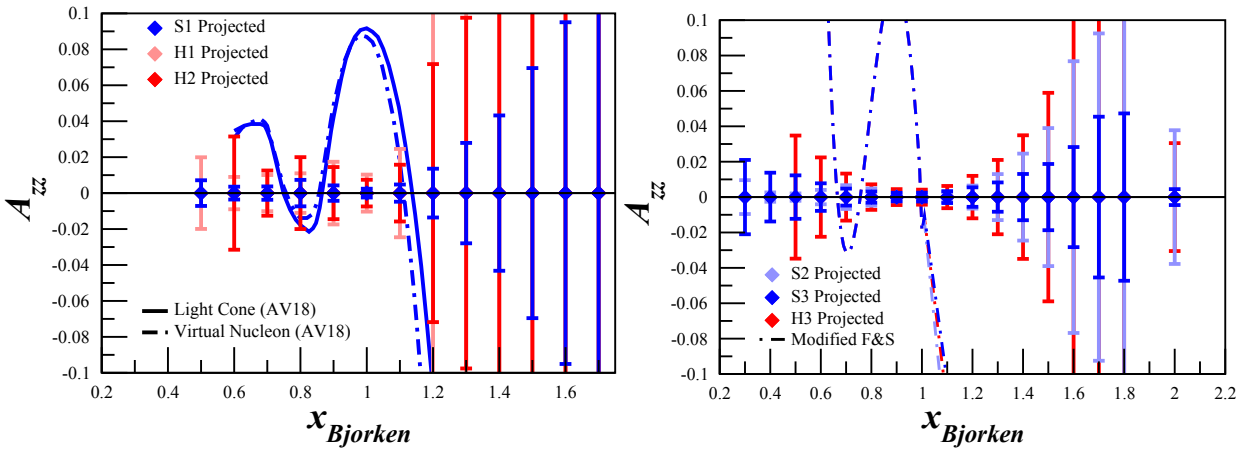

Figure 11: Projected uncertainties for the tensor asymmetry A_{zz} with 34 days of beam time, same as in Figure 10, but zoomed in to $-0.1 < A_{zz} < 0.1$ to more clearly show the small uncertainties around the quasi-elastic peak.

	S2: $Q^2 = 0.7$ (GeV/c)^2			H3: $Q^2 = 0.3$ (GeV/c)^2			S3: $Q^2 = 0.2$ (GeV/c)^2		
x	f_{dil}	δA_{zz}^{stat} $\times 10^{-2}$	δA_{zz}^{sys} $\times 10^{-2}$	f_{dil}	δA_{zz}^{stat} $\times 10^{-2}$	δA_{zz}^{sys} $\times 10^{-2}$	f_{dil}	δA_{zz}^{stat} $\times 10^{-2}$	δA_{zz}^{sys} $\times 10^{-2}$
0.30	0.24	0.99	1.84	—	—	—	0.18	2.13	1.84
0.40	0.28	0.26	1.84	—	—	—	0.12	1.38	1.84
0.50	0.32	0.21	1.84	0.14	3.52	1.84	0.11	1.23	1.84
0.60	0.19	0.41	????	0.12	2.26	????	0.18	0.78	????
0.70	0.13	0.68	????	0.18	1.33	????	0.28	0.48	????
0.80	0.19	0.48	0.48	0.30	0.72	0.48	0.42	0.31	0.48
0.90	0.39	0.22	1.10	0.46	0.45	1.10	0.54	0.24	1.10
1.00	0.52	0.16	????	0.52	0.43	????	0.58	0.25	????
1.10	0.39	0.28	1.27	0.43	0.63	1.07	0.53	0.33	0.95
1.20	0.22	0.65	2.54	0.30	1.15	2.14	0.40	0.55	1.91
1.30	0.14	1.34	3.81	0.19	2.16	3.22	0.32	0.83	2.87
1.40	0.09	2.29	5.06	0.14	3.52	4.29	0.24	1.31	3.82
1.50	0.06	4.09	6.35	0.10	5.85	5.37	0.20	1.86	4.78
1.60	0.04	7.76	7.60	0.06	10.4	6.45	0.14	2.87	5.74
1.70	0.04	9.23	8.88	0.05	13.5	7.52	0.10	4.53	6.69
1.80	0.03	14.9	9.20	0.06	13.9	8.60	0.11	4.73	7.66
2.00	0.67	3.79	9.20	0.20	3.05	9.20	0.70	0.45	9.20

Table 5: Summary of the expected uncertainty for each x bin for settings S2, S3, and H3.

Setting	Q^2 (GeV^2)	δT_{20}^{stat} $\times 10^{-2}$	δT_{20}^{sys} $\times 10^{-2}$
H2	1.8	13.2	4.7
S1	1.5	3.95	4.6
S2	0.7	5.36	4.6
H3	0.3	4.31	9.2
S3	0.2	0.64	5.5

Table 6: Expected uncertainties for T_{20}, assuming a systematic uncertainty of 9.2%, which could be reduced further by utilizing the S3 measurement as a calibration for the polarized target.

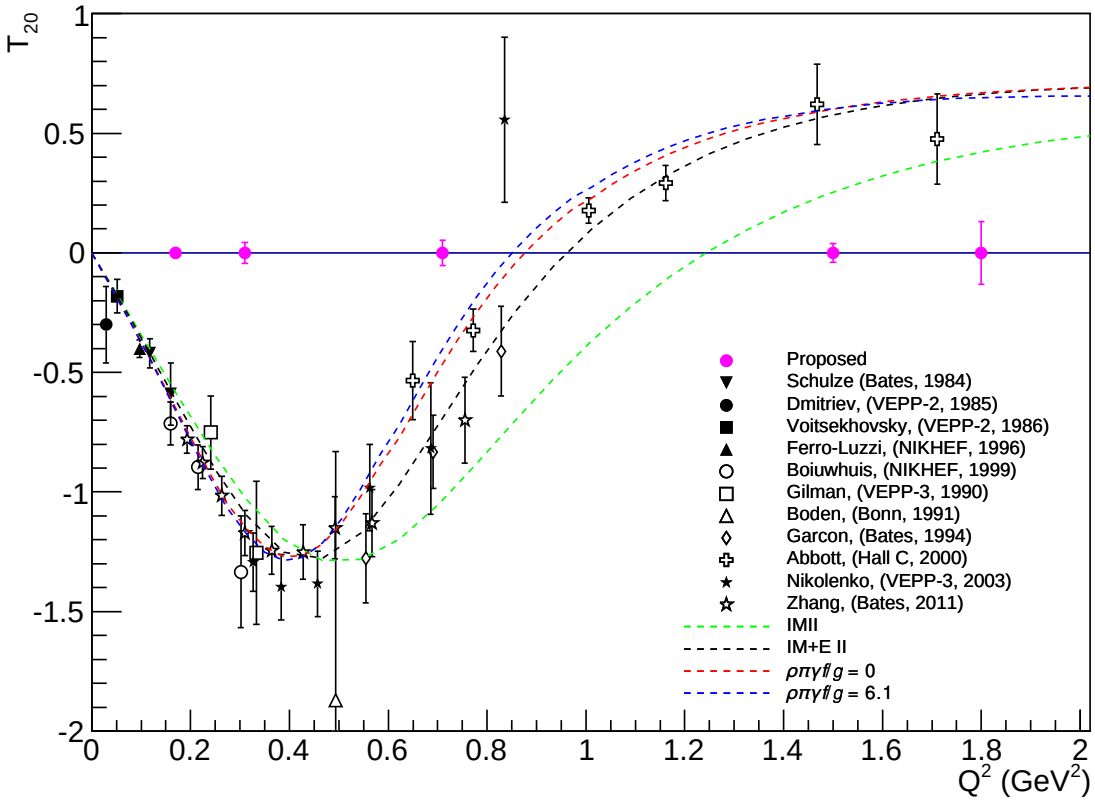

Figure 12: Projected uncertainties for the elastic tensor analyzing power T_{20} with 34 days of beam time.

and the object of ongoing studies. A unique feature of the measurement proposed here is that it selects small-size configurations in the deuteron both through the tensor asymmetry (D-state) and the choice of kinematics ($x > 1$), amplifying the overall effect. The use of $x > 1$ for selecting small-size NN configurations has been demonstrated in previous studies of deep-inelastic structure.

The measurement proposed here arises from a well-developed context, presents a clear objective, and enjoys strong theory support. It would further explore the nature of short-range pn correlations in nuclei, the discovery of which has been one of the most important results of the JLab 6 GeV nuclear program. Development of a full proposal should be encouraged."

4.2 Technical Advisory Committee

"This experiment utilizes the same apparatus and techniques as the conditionally approved b1 experiment C13-12-011. The comments in the TAC report for that experiment also apply to this experiment.

The requirement to understand and mitigate time-dependent systematic effects may be less as the asymmetry A_{zz}, at least for $x > 1$, is expected to be larger than for b1. However, measuring with $\delta A_{zz} < 0.10$ still requires a systematic control of the raw asymmetry to better than 1%. This is still challenging with a target polarization that is cycled on and off about once a day. Furthermore, at $x > 1$, short range structure enhances inclusive cross sections in nuclei relative to deuterium. This will reduce the dilution factor for $x > 1$ measurements, reducing the raw asymmetries to levels where understanding and controlling systematic errors will still be important."

4.3 Program Advisory Committee

"**Measurement and Feasibility:** Electron scattering off tensor-polarized deuterium would be measured in the quasi-elastic region using the Hall C HMS and SHMS spectrometers. This proposal would use the same setup as the C1-approved experiment E12-13-011, which is to measure the deuteron tensor structure function b1. The C1-approval is subject to demonstration that 35% tensor polarization is possible. The expected asymmetry is larger in the case of this measurement, but we anticipate that a similar requirement would apply. It is anticipated that a full proposal would be for 39 days, which would include 30 days for three different Q^2 values and 9.1 additional days of overhead.

Issues: A significant amount of beam time will be required for this measurement. A full proposal will need a detail discussion of expected systematic and statistical errors similar to what is in the letter that carefully justifies the requested time. The proposal should also demonstrate what sensitivity they will have to NN interaction models, such as the 6-quark model, final state interaction models, and NN interaction models,

mentioned in the proposal. It will also be important to discuss how the results will distinguish between effects from the NN-interaction, the treatment of these interactions at high virtuality, and the intrinsic deuteron wave function.

Recommendation: Proceed to proposal addressing the issues noted above."

4.4 Response to PAC42 Concerns

The tensor polarization of 30% used in the rates for this proposal is the same as condition on the E12-13-011 proposal, which was incorrectly mentioned as 35%. To ensure that the target is not significantly affected by the electron beam, we've estimated a current of 90 nA, as opposed to the 115 nA beam for b_1. We have expanded upon our estimated statistical and systematic uncertainties in Section 3.6 and in a recent technical note [citation needed], where we stress that a measurement of A_{zz} in the $x > 1$ region is ideal for understanding time-dependent systematic effects without significantly affecting the measurement. Furthermore, we will be measuring T_{20} at low Q^2 where it is well understood both experimentally and theoretically, which can be used as a calibration to reduce our leading systematics from understanding the target polarization. However, for the uncertainty calculations in this proposal we retain a conservative estimate of 12%.

Since PAC42, we have engaged a number of theorists who have provided models not only between light cone and virtual nucleon models, but also using different NN interaction potentials [19] and final state interactions [citation needed]. Furthermore, A_{zz} calculations are being performed at low Q^2 and are expected to be completed within a year [citation needed]. Although our measurements will be at too low W^2 to probe 6-quark, hidden color effects through an extraction of b_1, they are ideal for making a simultaneous measurement of T_{20} to test existing calculations at large Q^2, as discussed in Section 3.2, including in the region where recent Hall A and Hall C data show a discrepancy.

5 Summary

We have investigated the possibility of making high precision measurements of the quasi-elastic tensor asymmetry A_{zz}. By covering the kinematic range from the QE peak ($x = 1$) up to elastic scattering ($x = 2$), we expect that this data will provide valuable new insights about the high momentum components of the deuteron wavefunction. We are actively working with several theorists to get state-of-the-art calculations of light cone, virtual nucleon, and six-quark models. Additional calculations are being performed that include final-state interactions, and low Q^2 sensitivity to NN potentials. It is important to note that this is the same kinematic region that has been shown to be correlated with the EMC effect via the $x > 1$ A/D (e, e') results.

We have found that with 34 days of beam and an additional 10.3 days of overhead, A_{zz} can be measured with high precison at $Q^2 = 1.5$, 0.7, and 0.3 $(\mathrm{GeV}/c)^2$ in Hall C using identical equipment as the upcoming b_1 measurement while being less sensitive to systematic uncertainties. In addition, it will fill a gap in measurements of A_{zz} between the $T_{20} \propto A_{zz}$ elastic measurements and the $b_1 \propto \frac{A_{zz}}{F_1^d}$ deep-inelastic measurements.

References

[1] L. Frankfurt and M. Strikman, Phys.Rept. **160**, 235 (1988).

[2] M. Sargsian, private communication, to be published.

[3] J. L. Forest *et al.*, Phys. Rev. **C54**, 646 (1996).

[4] J. Arrington, D. Higinbotham, G. Rosner, and M. Sargsian, Prog.Part.Nucl.Phys. **67**, 898 (2012).

[5] W. Van Orden, private communication.

[6] M. Garcon and J. Van Orden, Adv.Nucl.Phys. **26**, 293 (2001).

[7] L. L. Frankfurt and M. I. Strikman, Phys. Rept. **76**, 215 (1981).

[8] L. Frankfurt, M. Strikman, D. Day, and M. Sargsian, Phys.Rev. **C48**, 2451 (1993).

[9] J. Arrington, C. Armstrong, T. Averett, O. K. Baker, L. de Bever, *et al.*, Phys.Rev.Lett. **82**, 2056 (1999).

[10] N. Fomin, J. Arrington, R. Asaturyan, F. Benmokhtar, W. Boeglin, *et al.*, Phys.Rev.Lett. **108**, 092502 (2012).

[11] S. Veerasamy and W. N. Polyzou, Phys. Rev. C **84**, 034003 (2011).

[12] F. Gross, Phys.Rev. **C26**, 2203 (1982).

[13] W. Buck and F. Gross, Phys.Rev. **D20**, 2361 (1979).

[14] L. Frankfurt and M. Strikman, Nucl.Phys. **B148**, 107 (1979).

[15] L. Alexa *et al.*, Phys.Rev.Lett. **82**, 1374 (1999).

[16] J. Van Orden, N. Devine, and F. Gross, Phys.Rev.Lett. **75**, 4369 (1995).

[17] M. M. Sargsian, Phys.Rev. **C82**, 014612 (2010).

[18] F. Gross and A. Stadler, Phys.Rev. **C82**, 034004 (2010).

[19] M. M. Sargsian and M. I. Strikman, J.Phys.Conf.Ser. **543**, 012009 (2014).

[20] M. Sargsian, private communication.

[21] M. Strikman, private communication.

[22] S. Liuti, private communication.

[23] G. Miller, private communication.

[24] W. Cosyn, private communication.

[25] The Madison Convention, *Proceedings of the 3rd International Symposium on Polarization Phenomena in Nuclear Reactions*, edited by H. H. Barschall and W. Haeberli (The Unviersity of Wisconsic Press, Madison) 1970, p. XXV.

[26] B. Boden, V. Burkert, G. Knop, G. Kroesen, M. Leenen, *et al.*, Z.Phys. **C49**, 175 (1991).

[27] C. Keith, JLab polarized target group. Private communication.

[28] W. Meyer *et al.*, Nucl. Instrum. Meth. **A244**, 574 (1986).

[29] C. Dulya *et al.*, Nucl. Instrum. Meth. **A398**, 109 (1997).

[30] P. Bosted and V. Mamyan, e-print **arXiv:1203.2262**, (2012).

[31] D. Keller, Nucl. Inst. and Meth. **A728**, 133 (2013).

[32] D. Keller, XVth International Workshop on Polarized Sources, Targets, and Polarimetry **PoS(PSTP2013)010**, (2013).

[33] E. Long *et al.*, JLab Technical note, JLAB-TN-13-029 (2013).

[34] L. Frankfurt, M. Sargsian, and M. Strikman, Int.J.Mod.Phys. **A23**, 2991 (2008).